ARCHIVE OF MECHANICAL ENGINEERING

DOI: 10.24425/ame.2025.154736 2025, Vol. 72, No. 2, pp. 249–269

Krzysztof MAGNUCKI [1], Piotr KĘDZIA [2], Iwona WSTAWSKA [2]

Elastic buckling of a two-part beam on Winkler's elastic foundation

Received 18 January 2025, **Revised** 22 April 2025, **Accepted** 29 April 2025, **Published online** 29 May 2025

Keywords: stability, two-part beam, elastic foundation, sandwich beam, critical loads

This paper is devoted to the behavior of an axially compressed two-part beam resting on elastic foundation. The beam was composed of two parts: rigid homogeneous part and sandwich three-layered part. The analytical model of the beam on the elastic foundation has been prepared. Winkler model has been assumed for the foundation description. Moreover, original function of deflection has been introduced and employed by the authors. The critical loads as a function of geometric and mechanical properties of the two-part beam and the parameters of Winkler's foundation were calculated. In addition, numerical analysis has been performed. Sample analytical and numerical calculations have been carried out, demonstrating good compatibility between the results attained with both models. The numerical analysis included the critical loads calculations for the beam with and without the elastic foundation. In both cases, the difference between analytical and numerical values of the critical loads did not exceed 8%.

1. Introduction

Multi-layered structures appeared in the second half of the 20th century, along with the problem of their stability. The development of technologies, related to the production of three-layered structures, facilitated their wide application. Designing of these elements allowed for the optimization of analytical and numerical methods. The continued advance of modern composite materials is forcing researchers to develop ever simpler and more useful tools for designing and manufacturing these components. Unfortunately, development of methods essential for the accurate

✉ Iwona WSTAWSKA, e-mail: iwona.wstawska@put.poznan.pl

[1]Łukasiewicz Research Network – Poznan Institute of Technology, Poznan, Poland

[2]Poznan University of Technology, Poznan, Poland

design of composite structures is not a straightforward task, and this is primarily related to their properties. The characteristics of composites are heterogeneity and anisotropic properties.

The characteristics of three-layered beams subjected to disparate loads, as well as the mechanisms associated with their failure, can be determined after simple axial compression or bending tests. For the first case of compressive load, sandwich structures may buckle either globally or locally. Local buckling is one of the most common problems appearing in sandwich structures due to the fact that the faces are much thinner that the core and therefore they have to resist the same values of load as the core itself. Loaded face behaves like a beam, plate or shell on an elastic foundation (core). It causes that the core is not subjected to significant local deformations, which leads to high values of shear and normal stresses. This may contribute to the formation of weak spots in the structure, which essentially accelerates its failure. Comparable results can be obtained for structures with a complex shape (e.g., cross-section of a cylindrical shell), even for simple cases of loads, i.e., constant internal pressure. It is advisable to use the principle of minimum potential energy for solving the equations related to multi-layered structures that are complex due to the character of loads, boundary conditions, changes in geometry, etc. Applying this approach, one can obtain appropriate solutions that can be verified in several ways.

Research related to buckling of sandwich beams has been conducted by several authors. Effective design of a simply-supported sandwich beam with a metal foam core has been analyzed by Magnucka-Blandzi and Magnucki [1]. They assumed that mechanical properties of the core varied in the depth direction. The stress state and critical force were considered, taking into account the theorem of minimum total potential energy. The studies revealed that the improvement of mechanical properties of the faces, relative to the parameters of the core, entail decreasing of the effective thicknesses of the faces as well as the effective irregularity of the core [1]. In addition, an effective design criterion of sandwich beam has been formulated by the authors. Strength and buckling of a five-layered sandwich beam subjected to axial compression or bending has been investigated by Magnucki et al. [2]. The faces of the sandwich beam were made of aluminum sheets and the core was manufactured from an aluminum foam. Moreover, two thin binding glue layers were incorporated between the faces and the core. Analytical, numerical, and experimental analyses were taken into the consideration. Good agreement between the values of buckling loads obtained from analytical and numerical studies was observed. Furthermore, good convergence between the values of normal and shear stresses was observed. Experimental analysis confirmed the correctness of analytical and numerical models used for an axially compressed beam [2]. Buckling analysis of functionally graded (FG) sandwich beams with various boundary conditions has been studied by Nguyen et al. [3]. A quasi-3D shear deformation theory has been introduced and employed by the authors. Two types of beams were prepared for the numerical analysis: FG faces + ceramic core and FG core

+ homogeneous faces. The influence of, inter alia, boundary conditions as well as faces and core thicknesses ratio on the values of critical buckling loads were examined. It was found that the theory proposed by the authors is applicable for buckling analysis of functionally graded sandwich beams. In addition, the obtained results were similar to those found in the literature. Buckling of a simply-supported unsymmetrical sandwich beam has been described by Magnucki et al. [4]. Analytical and numerical studies were conducted. The equations of motion were derived with the use of the Hamilton's principle. The beam was subjected to uniformly distributed transverse load or axial compressive force. The face layers varied in thickness and material properties. The discrepancies in results for two methods (analytical and numerical) were negligible, which may prove the correctness of the proposed models. Moreover, it was stated that the values of critical load depend on the position of the neutral axis [4]. Numerical model for buckling of a functionally graded sandwich beam has been performed by Liu et al. [5]. The scale boundary finite element method (SBFEM) has been proposed by the authors. The material properties of each layer altered in the thickness direction. The authors conceded that the values of critical buckling loads increase with the increase of face-core-face ratios thickness. It was also confirmed that boundary conditions play a significant role in the buckling response of a sandwich beam. The increase of critical buckling loads was observed with a simultaneous increase of constraints. Buckling analysis of sandwich composite beams based on higher-order refined zigzag theory has been carried out by Chen and Chen [6]. Various boundary conditions were taken into the consideration for numerical analysis. Critical loads as well as buckling modes were determined by the authors. It was affirmed that the values of buckling loads are associated with modifications of boundary conditions, aspect ratios, and thickness ratios [6]. Buckling of functionally graded curved sandwich beams has been presented by Lezgy-Nazargah et al. [7]. Global-local refined shear deformation theory has been adopted in this work. Material properties of the beams varied in the thickness direction. Results attained by the authors were compared with those from numerical methods and other higher-order beam theories. Detailed analysis of the problem made it possible to formulate the following conclusions: the increase of arc-length-to-thickness ratio induces the increase of buckling loads, the increase of radius of curvature-to-length ratio leads to a decrease of critical buckling loads [7]. Buckling analysis of sandwich curved structures has also been performed in [8–13]. Buckling of FG sandwich nanobeams with auxetic honeycomb core has been discussed by Lieu et al. [14]. Third-order shear deformation theory has been introduced and employed for the calculations. The influence of nanobeams geometrical parameters, as well as materials and boundary conditions on critical buckling loads was considered. It was concluded that the highest value of buckling load was achieved for an angle α (the angle between two adjacent walls in a honeycomb cell) approximately equal to 90°. This opinion allows us to deduce that for certain values of α the beam can withstand a compressive force of higher values. Numerical buckling studies of sandwich composite panels have

been prepared by Cara et al. [15]. Global buckling, as well as short-wavelength wrinkling of the faces were taken into account by the authors. The proposed model was assumed to be an accessible tool for multi-layered structures analysis. The influence of manufacturing parameters on buckling of sandwich composite structures with a honeycomb core has been formulated by Diniz et al. [16]. Two various types of the core (aramid and polypropylene materials) and four different types of faces (carbon, glass, glass/aramid hybrid, and carbon/aramid hybrid) were taken into account. The lowest values of buckling loads were acquired for two kinds of sandwich structures: with glass face and aramid core as well as glass face and polypropylene core. Further part of the research included, inter alia, the influence of variable boundary conditions on buckling loads. The analysis implemented by the authors allowed them to select the most optimal sandwich structure with a corrugated core.

Buckling of sandwich beams has also been presented in other works. Experimental and analytical studies of functionally graded carbon nanotube-reinforced sandwich beams have been prepared by Madenci et al. [17]. Good convergence between two adopted methods was observed. The influence of porosity and viscoelastic boundary conditions on buckling of FG sandwich beams in thermal environment has been analyzed by Patil et al. [18]. It was revealed that the occurrence of porosities improves buckling response of the structure. A new accurate analytical buckling model of sandwich panels/beams has been proposed by Cao and Niu [19]. Transverse shear deformation of the face was taken into account in calculations. Flexural buckling of sandwich beams with non-uniform sectional properties (affected by non-uniform temperature distribution in the beam cross-section) has been considered by Chen et al. [20]. The formula for critical buckling load, with and without the influence of transverse shear deformation, was introduced and employed in this work. A new multi-scale model for global buckling and local warping of sandwich beams has been examined by Mhada and Bourihane [21]. The coupling between local and global instabilities was taken into account in numerical calculations. The presented 2D model may be useful in the analysis of instability problems related to 2D sandwich structures subjected to compression. Buckling of a cenosphere reinforced epoxy composite core sandwich beam with sisal fabric/epoxy composite faces has been described by Waddar et al. [22]. The studies aimed to determine the influence of cenosphere loading and surface modification on critical buckling load. Sandwich beams with treated cenosphere/epoxy foam core were characterized by higher values of buckling loads, in contrast to untreated structures. Buckling analysis of thin-walled functionally graded sandwich box beams, under disparate boundary conditions, has been carried out by Lanc et al. [23]. Numerical model presented by the authors made it possible to prepare global buckling characteristics of functionally graded box beam type constructions. Experimental and numerical analysis of the influence of interfacial root crack on the lateral buckling of a cantilever sandwich composite beam has been performed by Kiral et al. [24]. They noticed good agreement between two models they applied. It was confirmed that

the increase of a crack length induces the decrease of lateral buckling loads. Elastic buckling of isotropic laminated composite and sandwich beams has been studied by Karamanli and Aydogdu [25]. Shear and normal deformable beam theory was implemented for numerical analysis. It was stated that the type of an axially variable in-plane load and boundary conditions affect the values of critical buckling loads. Buckling analysis of sandwich beams with compliant interfaces has been discussed by Volokh and Needleman [26]. The authors affirmed that compliant interfaces lead to a significant decrease of a bifurcation load.

The character of beam-foundation interaction is a substantial feature that also affects the values of critical buckling loads. The assumption of beams on elastic foundation was originally presented by Winkler. The beam rests on elastic foundation where, under the applied external loads, the reaction forces of the foundation are proportional at every point to the deflection of the beam at this point. Buckling of functionally graded sandwich Timoshenko beams resting on nonlocal elastic foundation has been considered by Zhang et al. [27]. The beam was made of functionally graded faces and a homogeneous core. The equations of motion and boundary conditions were assumed based on Hamilton's principle. The studies led to the following conclusions: an increase of nonlocal parameters affects buckling loads of sandwich beams, and critical buckling loads decrease with the increase of FG gradient index value (for all boundary conditions and cross-sections). A two-layered functionally graded sandwich curved beam resting on Winkler-Pasternak elastic foundation has been analyzed by Nguyen Thi [28]. The simply-supported beam was composed of two layers connected together with the use of shear connectors. The influence of mechanical and geometrical parameters of curved beams was taken into the consideration by the authors. It was found that higher values of mechanical buckling stress appear in the beam with mechanical properties varying according to the Voigt's model law, rather than the Mori-Tanaka model [28]. Thermal buckling of a truss core sandwich panel resting on a two-parameter elastic foundation has been investigated by Fu et al. [29]. The Reissner plate theory and first-order shear deformation theory were adopted to model the response of the structure. It was concluded that the critical buckling temperature increased with the increase of a radius and foundation stiffness parameters values, as well as the height of a truss core. Furthermore, the influence of shear foundation stiffness on critical buckling temperature was greater than that of Winkler foundation stiffness [29]. Buckling analysis of a three-layered rectangular nanocomposite microplate resting on Winkler-Pasternak elastic foundation has been carried out by Abbaspour and Arvin [30]. The plate was subjected to thermo-electro-mechanical load and made of a laminated nanocomposite core, reinforced with graphene platelets, as well as two piezoelectric faces. Thermo-electric and electro-mechanical buckling analysis was performed. The effect of, inter alia, boundary conditions, external applied voltage, and elastic foundation parameters were taken into the consideration for calculations. It was revealed that the types of boundary conditions, the graphene platelet dispersion pattern and weight fraction as well as the applied voltage affect

the thermal/mechanical buckling load. Introducing an elastic foundation into the structure changes its behavior. The occurrence of the elastic foundation causes that the increment percent in the thermal and shear mechanical buckling loads is not affected by the graphene platelets dispersion pattern [30]. Thermal buckling characteristics of edge-cracked functionally graded multi-layered graphene nanocomposite beams resting on Pasternak elastic foundation has been presented by Song et al. [31]. It was revealed, inter alia, that thermal buckling temperature changes decrease with the increase of the crack length. Furthermore, the increase of Winkler or shearing layer reduces the sensitivity of thermal buckling response of beams to the crack [31]. Nonlinear static buckling analysis of magneto-electro-elastic sandwich plate has been formulated by Quang et al. [32]. The plate was resting on Pasternak elastic foundation and subjected to mechanical, electrical, and magnetic loads. The sandwich structure consisted of an auxetic honeycomb core and two faces made of magneto-electro-elastic material. The influence of, inter alia, elastic foundation, temperature, and geometrical parameters on buckling response of the structure was taken into account by the authors. It was found that the increase in temperature, as well as the increase in two elastic foundation coefficients, increases the values of critical buckling loads [32]. Buckling analysis of a porous tapered plate composed of functionally graded materials and resting on Pasternak foundation has been studied by Kumar et al. [33]. It was found that the parameters of elastic foundation and porosity of the plate affect the stability of the structure. The occurrence of porosity decreases the values of buckling loads. The main conclusions from this work are as follows: the values of buckling loads increase with the increase of clamped boundary constraints, the increase of taper ratio induces the increase of buckling loads, the increase of elastic foundation stiffness entails the increase of buckling loads [33]. Thermal buckling of sandwich panels in supersonic airflow with a pyramidal lattice core and resting on elastic foundations has been examined by Chai et al. [34]. The authors described the effect of geometric parameters as well as the parameters of elastic foundation on the structure stability. It was assumed that the change in critical thermal buckling temperature decreases with the increase of aspect ratio. In addition, thermal buckling bound increases with the increase of the inclination angle [34]. It was also noticed that the stability characteristics can be adjusted by changing the values of shearing layer parameters. Stability of an axially compressed three-layered beam resting on elastic foundation has been described by Wstawska et al. [35]. The influence of variable elastic foundation parameters as well as geometric and mechanical properties of the sandwich beam on buckling loads were discussed. The authors revealed a significant influence of elastic foundation parameters on critical buckling loads. Moreover, the thickness of the core also played a meaningful role in buckling response of the beam. Symmetric thermal buckling of an annular sandwich plate resting on Pasternak foundation has been proposed by Yang et al. [36]. The plate was composed of two asymmetric piezoelectric faces and a graphene-platelets-reinforced composite core (GPLRC). The equations used by the authors were based on first-

order shear deformation theory, whereas the governing equations were prepared based on Hamilton's principle and Maxwell's static electricity equations. Disparate boundary conditions were introduced and employed. It was attained that the critical buckling temperature rise decreases with the decrease of graphene-platelets weight fraction.

Buckling of sandwich beams on elastic foundation has also been presented in some other works. Thermal buckling and postbuckling of composite beams reinforced with functionally graded multilayer graphene platelets and resting on nonlinear elastic foundations has been prepared by Lv et al. [37]. The influence of, inter alia, axial force, boundary conditions, slenderness ratio, and elastic foundation parameter on thermal buckling and postbuckling was investigated. Thermal postbuckling of porous sandwich beams with graphene platelets reinforcements resting on elastic foundations has been analyzed by Chen et al. [38]. Nonlinear studies were carried out by the authors. Dynamic buckling analysis of a graphene platelet reinforced sandwich functionally graded porous plate has been considered by Li et al. [39]. The plate was resting on Winkler-Pasternak elastic foundation. Main conclusions from this work are as follows: the initial imperfection of the plate induces the decrease of buckling load, the increase of environment temperature entails a certain increase of buckling load, the increase of elastic foundation parameters causes the increase of buckling load, the values of buckling loads decrease with the increase of core porosity [39]. Nonlinear snap-buckling of an infinitely long nanocomposite cylindrical panel resting on nonlinear elastic foundation has been examined by Babaei [40]. The author revealed that the span-buckling intensity increases with the increase of panel geometrical parameters. In addition, the boundary conditions also play a substantial role in snap-buckling response of the structure [40]. Static buckling and post-buckling dynamic analysis of a functionally graded pipeline with geometric imperfections and resting on Pasternak foundation has been proposed by Chang et al. [41]. Numerical calculations confirmed that Pasternak foundation has a meaningful influence on critical buckling load and post-buckling structure. Buckling of composite conical shells reinforced with carbon nanotubes and resting on a two-parameter elastic foundation has been studied by Sofiyev and Kuruoglu [42]. The shells were subjected to a hydrostatic pressure and axial compression. The analysis allowed one to determine the combined buckling loads. Examination of web buckling in web core panels under a distributed load has been carried out by Briscoe et al. [43]. First, isotropic buckling model of the plate on Pasternak foundation was implemented in this work. Subsequently, the developed model was adopted for buckling analysis of web core sandwich panels. Stability of sandwich functionally graded porous plates reinforced with graphene platelets in subsonic flow and resting on Winkler-Pasternak foundation has been described by Wang and Yao [44]. The structure was composed of a porous core and two metal faces. It was shown that by decreasing the porosity or increasing the surface thickness ratio and elastic foundation parameters one can ameliorate the stability response of the plates [44]. Buckling

of elastically connected parallel-beams subjected to a compressive axial loading has been discussed by Kozić et al. [45]. The beams were simply supported and continuously joined by a Kerr-type three-parameter layer. The effect of a compressive axial load ratio on a critical buckling load was analyzed. Three-dimensional buckling of composite nanoplates with a coated one-dimensional quasicrystal has been studied by Guo et al. [46]. The structure being examined was embedded in an elastic medium and subjected to uniaxial and biaxial compression. Pasternak-type model was introduced for the analysis to describe the interaction between the nanoplates and the elastic medium. It was concluded that the values of critical buckling loads were lower for biaxial compression than those obtained for the uniaxial one [46].

In this work, elastic buckling of an axially compressed two-part beam on Winkler's elastic foundation has been examined. The axially compressed beam consisted of a rigid and a sandwich part (three-layered symmetrical part). The analytical model, presented in Section 2, allowed us to determine the values of critical buckling loads as well as buckling modes. The numerical model allowed us to confirm the correctness of mathematical solution and validate the calculations.

The outline of the following part of the paper is as follows: in Section 2, an analytical model of a two-part beam on Winkler's elastic foundation is described taking into account the variable parameters of elastic foundation; in Section 3, comparative studies are carried out, and analytical and numerical results are taken into the consideration; finally, the last Section contains conclusions.

2. Analytical model of the beam

The subject of the paper is a simply supported beam of length L resting on an elastic foundation (Fig. 1). The width of this beam is b, thicknesses of the faces are h_f, and thickness of the core is h_c. The beam considered in this paper is subjected to a compressive axial load F_0 and consists of two parts:

- first part – rigid part of length L_0 and depth h,
- second part – sandwich part of length L_s and total depth $h = h_c + 2h_f$.

Total length of this beam is equal $L = L_0 + L_s$.

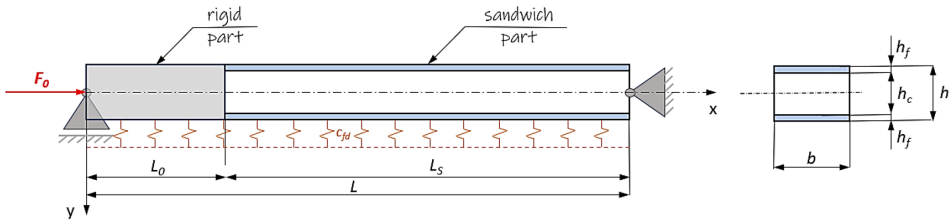

Fig. 1. Scheme of the two-part beam

According to paper [47], two differential equations of equilibrium of the classical sandwich part are as follows:

$$c_{vv}\frac{\mathrm{d}^4 v}{\mathrm{d}x^4} - c_{v\psi}\frac{\mathrm{d}^3\psi}{\mathrm{d}x^3} + 12\frac{c_{fd}}{E_f b h^3}\left[\frac{2}{3}v_0 + v(x)\right] + 12\frac{F_0}{E_f b h^3}\frac{\mathrm{d}^2 v}{\mathrm{d}x^2} = 0, \tag{1}$$

$$c_{v\psi}\frac{\mathrm{d}^3 v}{\mathrm{d}x^3} - c_{\psi\psi}\frac{\mathrm{d}^2\psi}{\mathrm{d}x^2} + c_{\psi}\frac{\psi(x)}{h^2} = 0, \tag{2}$$

where: $0 \leqslant x \leqslant L_s$, $b = \beta h$, $c_{vv} = 1 - (1 - e_c)\,\chi_c^3$, $c_{v\psi} = 3 - (3 - 2e_c)\,\chi_c^2$, $c_{\psi\psi} = 4\,[3 - (3 - e_c)\,\chi_c]$, $c_{\psi} = \dfrac{24}{1 + \nu_c}\dfrac{e_c}{\chi_c}$.

The system has been approximately solved. The function of deflection $v(x)$ is assumed in the following form (Fig. 2):

$$v(x) = v_0 \cos\left(\frac{\pi}{2}\frac{x}{L_s}\right) + v_a \sin\left(\pi\frac{x}{L_s}\right). \tag{3}$$

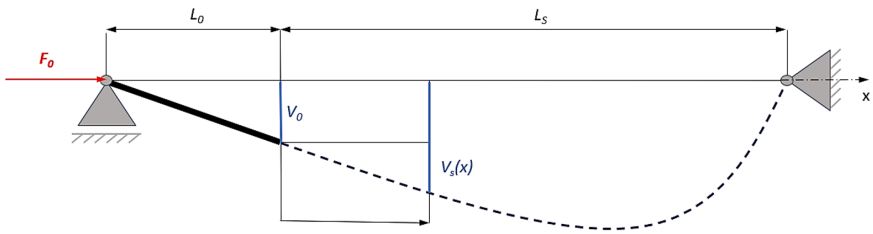

Fig. 2. Scheme of the buckling shape of the beam

The above function meets the following boundary conditions: $v(0) = v_0$, $v(L_s) = 0$, and the angle

$$\begin{aligned} \frac{\mathrm{d}v}{\mathrm{d}x} &= -\frac{\pi}{2}\frac{v_0}{L_s}\sin\left(\frac{\pi}{2}\frac{x}{L_s}\right) + \pi\frac{v_a}{L_s}\cos\left(\pi\frac{x}{L_s}\right), \\ \left.\frac{\mathrm{d}v}{\mathrm{d}x}\right|_0 &= \pi\frac{v_a}{L_s} = \frac{v_0}{L_0} \quad \Rightarrow \quad v_0 = \pi k_0 v_a\,, \end{aligned} \tag{4}$$

where the dimensionless coefficient $k_0 = L_0/L_s$.

This deflection function in the dimensionless coordinate $\xi = x/L_s$ is as follows

$$\begin{aligned} v(\xi) &= \left[\pi k_0 \cos\left(\frac{\pi}{2}\xi\right) + \sin(\pi\xi)\right] v_a\,, \\ \bar{v}(\xi) &= \pi k_0 \cos\left(\frac{\pi}{2}\xi\right) + \sin(\pi\xi)\,, \end{aligned} \tag{5}$$

where the subsequent derivatives of this function are:

$$\frac{\mathrm{d}v}{\mathrm{d}\xi} = \left[-\frac{\pi^2}{2}k_0 \sin\left(\frac{\pi}{2}\xi\right) + \pi\cos(\pi\xi)\right] v_a\,, \tag{6}$$

$$\frac{\mathrm{d}^2v}{\mathrm{d}\xi^2} = -\pi^2\left[\frac{\pi}{4}k_0 \cos\left(\frac{\pi}{2}\xi\right) + \sin(\pi\xi)\right] v_a\,, \tag{7}$$

$$\frac{\mathrm{d}^3v}{\mathrm{d}\xi^3} = \pi^3\left[\frac{\pi}{8}k_0 \sin\left(\frac{\pi}{2}\xi\right) - \cos(\pi\xi)\right] v_a\,, \tag{8}$$

$$\frac{\mathrm{d}^4v}{\mathrm{d}\xi^4} = \pi^4\left[\frac{\pi}{16}k_0 \cos\left(\frac{\pi}{2}\xi\right) + \sin(\pi\xi)\right] v_a\,. \tag{9}$$

Consequently, Eqs. (1) and (2) in this dimensionless coordinate have the form

$$c_{vv}\frac{\mathrm{d}^4v}{\mathrm{d}\xi^4} - c_{v\psi}\frac{\mathrm{d}^3\psi}{\mathrm{d}\xi^3}L_s + 12\frac{c_{fd}}{E_f}\frac{\lambda_s^4}{\beta}\left[\frac{2}{3}\pi k_0 + \bar{v}(\xi)\right] v_a + 12\bar{F}_0\lambda_s^2\frac{\mathrm{d}^2v}{\mathrm{d}\xi^2} = 0, \tag{10}$$

$$\begin{aligned} c_{v\psi}\frac{\mathrm{d}^3v}{\mathrm{d}\xi^3} - c_{\psi\psi}\frac{\mathrm{d}^2\psi}{\mathrm{d}\xi^2}L_s + c_\psi\lambda_s^2\psi(\xi)L_s = 0\,,\\ c_{\psi\psi}\frac{\mathrm{d}^2\psi}{\mathrm{d}\xi^2} - c_\psi\lambda_s^2\psi(\xi) = c_{v\psi}\frac{1}{L_s}\frac{\mathrm{d}^3v}{\mathrm{d}\xi^3}\,, \end{aligned} \tag{11}$$

where relative length of the sandwich part is $\lambda_s = L_s/h$, $\overline{F}_0 = F_0/E_f bh$, and $\beta = b/h$.

Equation (11), with consideration of the function (5), after simple transformation is as follows:

$$\frac{\mathrm{d}^2\psi}{\mathrm{d}\xi^2} - \frac{c_\psi}{c_{\psi\psi}}\lambda_s^2\psi(\xi) = \frac{c_{v\psi}}{c_{\psi\psi}}\pi^3\left[\frac{\pi}{8}k_0 \sin\left(\frac{\pi}{2}\xi\right) - \cos(\pi\xi)\right]\frac{v_a}{L_s}\,, \tag{12}$$

where the dimensionless coefficient $\alpha = \sqrt{c_\psi/c_{\psi\psi}}$.

The general solution of the Eq. (12) is in the following form:

$$\psi(\xi) = c_1\sinh(\alpha\lambda_s\xi) + c_2\cosh(\alpha\lambda_s\xi) + \left[c_{01}\sin\left(\frac{\pi}{2}\xi\right) - c_{02}\cos(\pi\xi)\right]\frac{v_a}{L_s}\,, \tag{13}$$

where the second derivative is in the following form:

$$\begin{aligned} \frac{\mathrm{d}^2\psi}{\mathrm{d}\xi^2} &= (\alpha\lambda_s)^2\left[c_1\sinh(\alpha\lambda_s\xi) + c_2\cosh(\alpha\lambda_s\xi)\right]\\ &\quad + \left[-c_{01}\frac{\pi^2}{4}\sin\left(\frac{\pi}{2}\xi\right) + c_{02}\pi^2\cos(\pi\xi)\right]\frac{v_a}{L_s}\,, \end{aligned} \tag{14}$$

and $c_{01} = -\dfrac{\pi^4}{2\left[\pi^2 + 4(\alpha\lambda_s)^2\right]}\dfrac{c_{v\psi}}{c_{\psi\psi}}k_0$, $c_{02} = -\dfrac{\pi^3}{\pi^2 + (\alpha\lambda_s)^2}\dfrac{c_{v\psi}}{c_{\psi\psi}}$.

After substituting the above c_{01} and c_{02} functions, Eq. (13) can be rewritten in the following form:

$$\psi(\xi) = c_1 \sinh(\alpha\lambda_s\xi) + c_2 \cosh(\alpha\lambda_s\xi) + \left\{ -\frac{\pi^4}{2\left[\pi^2+4(\alpha\lambda_s)^2\right]} \frac{c_{v\psi}}{c_{\psi\psi}} k_0 \sin\left(\frac{\pi}{2}\xi\right) + \frac{\pi^3}{\pi^2+(\alpha\lambda_s)^2} \frac{c_{v\psi}}{c_{\psi\psi}} \cos(\pi\xi) \right\} \frac{v_a}{L_s}, \tag{15}$$

$$\psi(\xi) = c_1 \sinh(\alpha\lambda_s\xi) + c_2 \cosh(\alpha\lambda_s\xi) + \frac{\pi^3}{2} \frac{c_{v\psi}}{c_{\psi\psi}} \left\{ -\frac{\pi}{\pi^2+4(\alpha\lambda_s)^2} k_0 \sin\left(\frac{\pi}{2}\xi\right) + \frac{2}{\pi^2+(\alpha\lambda_s)^2} \cos(\pi\xi) \right\} \frac{v_a}{L_s}.$$

Taking into account the boundary conditions: $\psi(0) = 0$, $\mathrm{d}\psi/\mathrm{d}\xi\big|_1 = 0$, one obtains two integration constants:

$$c_2 = -\frac{\pi^3}{\pi^2+(\alpha\lambda_s)^2} \frac{c_{v\psi}}{c_{\psi\psi}} \frac{v_a}{L_s}, \tag{16}$$

$$c_1 = -c_2 \tanh(\alpha\lambda_s), \tag{17}$$

where

$$\psi(0) = 0 \;\Rightarrow\; c_2 + \frac{\pi^3}{2} \frac{c_{v\psi}}{c_{\psi\psi}} \frac{2}{\pi^2+(\alpha\lambda_s)^2} \frac{v_a}{L_s} = 0$$

$$\Rightarrow\; c_2 = -\frac{\pi^3}{\pi^2+(\alpha\lambda_s)^2} \frac{c_{v\psi}}{c_{\psi\psi}} \frac{v_a}{L_s},$$

$$\frac{\mathrm{d}\psi}{\mathrm{d}\xi} = \alpha\lambda_s c_1 \cosh(\alpha\lambda_s\xi) + \alpha\lambda_s c_2 \sinh(\alpha\lambda_s\xi) + \frac{\pi^3}{2} \frac{c_{v\psi}}{c_{\psi\psi}} \left\{ -\frac{\pi^2}{2\left[\pi^2+4(\alpha\lambda_s)^2\right]} k_0 \cos\left(\frac{\pi}{2}\xi\right) - \frac{2\pi}{\pi^2+(\alpha\lambda_s)^2} \sin(\pi\xi) \right\} \frac{v_a}{L_s},$$

$$\left.\frac{\mathrm{d}\psi}{\mathrm{d}\xi}\right|_1 = 0 \;\Rightarrow\; \alpha\lambda_s\left[c_1\cosh(\alpha\lambda_s) + c_2\sinh(\alpha\lambda_s)\right] = 0 \;\Rightarrow\; c_1 = -c_2\tanh(\alpha\lambda_s).$$

Thus the function (12) is as follows

$$\psi(\xi) = c_2\left[-\tanh(\alpha\lambda_s)\sinh(\alpha\lambda_s\xi) + \cosh(\alpha\lambda_s\xi)\right] \frac{v_a}{L_s} + \frac{\pi^3}{2} \frac{c_{v\psi}}{c_{\psi\psi}} \left\{ -\frac{\pi}{\pi^2+4(\alpha\lambda_s)^2} k_0 \sin\left(\frac{\pi}{2}\xi\right) + \frac{2}{\pi^2+(\alpha\lambda_s)^2} \cos(\pi\xi) \right\},$$

$$\psi(\xi) = -\frac{\pi^3}{\pi^2+(\alpha\lambda_s)^2} \frac{c_{v\psi}}{c_{\psi\psi}} \left\{ \frac{\cosh\left[(1-\xi)\alpha\lambda_s\right]}{\cosh(\alpha\lambda_s)} - \cos(\pi\xi) + \frac{\pi}{2} \frac{\pi^2+(\alpha\lambda_s)^2}{\pi^2+4(\alpha\lambda_s)^2} k_0 \sin\left(\frac{\pi}{2}\xi\right) \right\} \frac{v_a}{L_s}. \tag{18}$$

Equation (10) with consideration of the expression (5) in the dimensionless coordinate is as follows

$$\begin{aligned}
&\pi^4 c_{vv}\left[\frac{\pi}{16}k_0\cos\left(\frac{\pi}{2}\xi\right)+\sin(\pi\xi)\right]v_a\\
&\quad-\frac{\pi^3}{\pi^2+(\alpha\lambda_s)^2}\frac{c_{v\psi}^2}{c_{\psi\psi}}\left\{(\alpha\lambda_s)^3\frac{\sinh\left[(1-\xi)\alpha\lambda_s\right]}{\cosh(\alpha\lambda_s)}+\pi^3\sin(\pi\xi)\right.\\
&\quad\left.+\frac{\pi^4}{16}\frac{\pi^2+(\alpha\lambda_s)^2}{\pi^2+4(\alpha\lambda_s)^2}k_0\cos\left(\frac{\pi}{2}\xi\right)\right\}v_a\\
&\quad+12\frac{c_{fd}}{E_f}\frac{\lambda_s^4}{\beta}\left\{\pi\left[\frac{2}{3}+\cos\left(\frac{\pi}{2}\xi\right)\right]k_0+\sin(\pi\xi)\right\}v_a\\
&\quad-12\pi^2\lambda_s^2\bar{F}_0\left[\frac{\pi}{4}k_0\cos\left(\frac{\pi}{2}\xi\right)+\sin(\pi\xi)\right]v_a=0.
\end{aligned}\tag{19}$$

This equation is solved using the Galerkin method, thus

$$\int_0^1 L(\xi)\bar{v}(\xi)\,\mathrm{d}\xi=0,\tag{20}$$

where $L(\xi)$ is the left part of the Eq. (19) and

$$\begin{aligned}
&\int_0^1\left[\frac{\pi}{16}k_0\cos\left(\frac{\pi}{2}\xi\right)+\sin(\pi\xi)\right]\left[\pi k_0\cos\left(\frac{\pi}{2}\xi\right)+\sin(\pi\xi)\right]\mathrm{d}\xi\\
&\qquad=\frac{1}{2}\left[1+\frac{17}{6}k_0+\frac{\pi^2}{16}k_0^2\right],
\end{aligned}\tag{21}$$

$$\begin{aligned}
&\int_0^1\left\{\frac{(\alpha\lambda_s)^3}{\cosh(\alpha\lambda_s)}\sinh\left[(1-\xi)\alpha\lambda_s\right]+\pi^3\sin(\pi\xi)\right.\\
&\quad\left.+\frac{\pi^4}{16}\frac{\pi^2+(\alpha\lambda_s)^2}{\pi^2+4(\alpha\lambda_s)^2}k_0\cos\left(\frac{\pi}{2}\xi\right)\right\}\left[\pi k_0\cos\left(\frac{\pi}{2}\xi\right)+\sin(\pi\xi)\right]\mathrm{d}\xi\\
&=\int_0^1\left\{\pi k_0\frac{(\alpha\lambda_s)^3}{\cosh(\alpha\lambda_s)}\sinh\left[(1-\xi)\alpha\lambda_s\right]\cos\left(\frac{\pi}{2}\xi\right)\right.\\
&\quad+\pi^4 k_0\sin(\pi\xi)\cos\left(\frac{\pi}{2}\xi\right)+\frac{\pi^5}{16}\frac{\pi^2+(\alpha\lambda_s)^2}{\pi^2+4(\alpha\lambda_s)^2}k_0^2\cos^2\left(\frac{\pi}{2}\xi\right)\\
&\quad+\frac{(\alpha\lambda_s)^3}{\cosh(\alpha\lambda_s)}\sinh\left[(1-\xi)\alpha\lambda_s\right]\sin(\pi\xi)+\pi^3\sin^2(\pi\xi)\\
&\quad\left.+\frac{\pi^4}{16}\frac{\pi^2+(\alpha\lambda_s)^2}{\pi^2+4(\alpha\lambda_s)^2}k_0\cos\left(\frac{\pi}{2}\xi\right)\sin(\pi\xi)\right\}\mathrm{d}\xi,
\end{aligned}\tag{22}$$

$$\int_0^1 \left\{\pi\left[\frac{2}{3}+\cos\left(\frac{\pi}{2}\xi\right)\right]k_0+\sin(\pi\xi)\right\}\left[\pi k_0\cos\left(\frac{\pi}{2}\xi\right)+\sin(\pi\xi)\right]\mathrm{d}\xi$$
$$=\frac{1}{2}\left[1+8k_0+\frac{\pi}{3}(3\pi+8)k_0^2\right], \tag{23}$$

$$\int_0^1 \left[\frac{\pi}{4}k_0\cos\left(\frac{\pi}{2}\xi\right)+\sin(\pi\xi)\right]\left[\pi k_0\cos\left(\frac{\pi}{2}\xi\right)+\sin(\pi\xi)\right]\mathrm{d}\xi$$
$$=\frac{1}{2}\left[1+\frac{10}{3}k_0+\frac{\pi^2}{4}k_0^2\right]. \tag{24}$$

After integration and complex transformation one obtains the dimensionless critical force in the form (integration of Eq. (19))

$$\pi^4 c_{vv}\frac{1}{2}\left[1+\frac{17}{6}k_0+\frac{\pi^2}{16}k_0^2\right]-\frac{\pi^3}{\pi^2+(\alpha\lambda_s)^2}\frac{c_{v\psi}^2}{c_{\psi\psi}}\pi\left\{\frac{\pi^2}{2}+\frac{(\alpha\lambda_s)^3}{\pi^2+(\alpha\lambda_s)^2}\tanh(\alpha\lambda_s)\right.$$
$$\left.+\frac{\left[\pi^2+(\alpha\lambda_s)^2\right]\left[17\pi^2+48(\alpha\lambda_s)^2\right]}{12\left[\pi^2+4(\alpha\lambda_s)^2\right]}k_0+\frac{\pi^4}{32}\frac{\pi^2+(\alpha\lambda_s)^2}{\pi^2+4(\alpha\lambda_s)^2}k_0^2\right\}$$
$$+12\frac{c_{fd}}{E_f}\frac{\lambda_s^4}{\beta}\frac{1}{2}\left[1+8k_0+\frac{\pi}{3}(3\pi+8)k_0^2\right]=12\pi^2\lambda_s^2\bar{F}_0\frac{1}{2}\left[1+\frac{10}{3}k_0+\frac{\pi^2}{4}k_0^2\right],$$

$$12\pi^2\lambda_s^2\bar{F}_0\left[1+\frac{10}{3}k_0+\frac{\pi^2}{4}k_0^2\right]=\pi^4 c_{vv}\left[1+\frac{17}{6}k_0+\frac{\pi^2}{16}k_0^2\right]$$
$$-\frac{\pi^4}{\pi^2+(\alpha\lambda_s)^2}\frac{c_{v\psi}^2}{c_{\psi\psi}}\left\{\pi^2+2\frac{(\alpha\lambda_s)^3}{\pi^2+(\alpha\lambda_s)^2}\tanh(\alpha\lambda_s)\right.$$
$$\left.+\frac{\left[\pi^2+(\alpha\lambda_s)^2\right]\left[17\pi^2+48(\alpha\lambda_s)^2\right]}{6\left[\pi^2+4(\alpha\lambda_s)^2\right]}k_0+\frac{\pi^4}{16}\frac{\pi^2+(\alpha\lambda_s)^2}{\pi^2+4(\alpha\lambda_s)^2}k_0^2\right\}$$
$$+12\frac{c_{fd}}{E_f}\frac{\lambda_s^4}{\beta}\left[1+8k_0+\frac{\pi}{3}(3\pi+8)k_0^2\right],$$

$$12\pi^2\lambda_s^2 k_F\bar{F}_0=\pi^4 c_{vv}k_v-\frac{\pi^4}{\pi^2+(\alpha\lambda_s)^2}\frac{c_{v\psi}^2}{c_{\psi\psi}}k_\psi+12\frac{c_{fd}}{E_f}\frac{\lambda_s^4}{\beta}k_{fd},$$

$$\overline{F_{0,\mathrm{CR}}}=\frac{\pi^2 c_{vv}}{12\lambda_s^2}\frac{k_v}{k_F}-\frac{\pi^2}{\pi^2+(\alpha\lambda_s)^2}\frac{k_\psi}{12\lambda_s^2 k_F}\frac{c_{v\psi}^2}{c_{\psi\psi}}+\frac{c_{fd}}{E_f}\frac{\lambda_s^2\cdot k_{fd}}{\pi^2\beta k_F}, \tag{25}$$

where

$$k_F = 1 + \frac{10}{3}k_0 + \frac{\pi^2}{4}k_0^2,$$

$$k_v = 1 + \frac{17}{6}k_0 + \frac{\pi^2}{16}k_0^2,$$

$$k_\psi = \pi^2 + 2\frac{(\alpha\lambda_s)^3}{\pi^2 + (\alpha\lambda_s)^2}\tanh(\alpha\lambda_s) + \frac{\left[\pi^2 + (\alpha\lambda_s)^2\right]\left[17\pi^2 + 48(\alpha\lambda_s)^2\right]}{6\left[\pi^2 + 4(\alpha\lambda_s)^2\right]}k_0 + \frac{\pi^4}{16}\frac{\pi^2 + (\alpha\lambda_s)^2}{\pi^2 + 4(\alpha\lambda_s)^2}k_0^2,$$

$$k_{fd} = 1 + 8k_0 + \frac{\pi}{3}(3\pi + 8)k_0^2.$$

Formula (25) presents the concept of critical load which depends on the values of elastic foundation parameters and geometrical parameters of the two-part beam. The values of critical loads for the beam with and without the presence of elastic foundation were taken into the consideration. For the beam without elastic foundation, k_0 geometrical parameter was adopted for calculations. For the beam with Winkler's elastic foundation, k_0, k_ψ, and k_{fd} played an essential role in the buckling response. The value of critical load appears for various values of these parameters, not necessarily for the same values.

Further part of this work presents the results of analytical studies. The values of critical buckling loads were calculated based on the model presented in Section 2. In addition, these values were compared with the results of numerical studies. A comparative investigation of the results acquired from those two methods was conducted.

3. Results and discussion

3.1. Analytical studies

Sample analytical values of critical loads in a function of variable parameters have been presented for the following data: $L = 500$ mm, $h = 20$ mm, $b = 20$ mm, $E_f = 72\,000$ MPa, $\nu_c = 0.3$, $c_{fd} = 0.5$ MPa, $e_c = 1/20$, $\chi_c = 17/20$, $\beta = 1$, $L_0 + L_s = L$, $\lambda_s = L_s/h$, $k_0 = L_0/L_s$.

First calculations were performed for the beam without the elastic foundation ($c_{fd} = 0$). The following values of k_0 (and λ_s) parameter were assumed: 2/3 (15), 3/7 (17.5), 1/4 (20), 1/9 (22.5), and 0 (25). The value 0 refers to the beam without the rigid part L_0 (a typical three-layered sandwich beam). In addition, in the special cases when $k_0 = 0$, $k_F = 1$, $k_v = 1$, $k_\psi = 0$, and $c_{fd} = 0$, Eq. (25) takes

the following form:

$$\overline{F_{0,\mathrm{CR}}} = \frac{\pi^2 c_{vv}}{12\lambda_s^2}\,. \tag{26}$$

The second part of research included the beam resting on Winkler's elastic foundation (c_{fd} = 0.5 MPa). The same values of k_0 and λ_s parameters were adopted (Table 1). Moreover, k_ψ and k_{fd} parameters were calculated and implemented for the analysis. The results of calculations are presented in Fig. 3.

Table 1. Results of analytical studies for variable beam parameters

Beam	Beam no. 1	Beam no. 2	Beam no. 3	Beam no. 4	Beam no. 5
λ_s	15.0	17.5	20.0	22.5	25.0
k_0	2/3	3/7	1/4	1/9	0
$F_{0,\mathrm{CR}}$ [kN] no foundation	20.812	17.891	16.281	15.551	15.396
$F_{0,\mathrm{CR}}$ [kN] with foundation	31.391	30.996	30.286	28.763	26.411

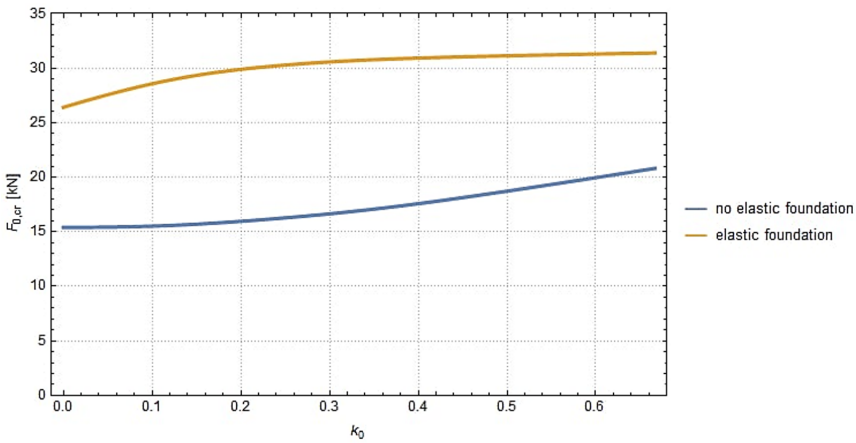

Fig. 3. The values of critical loads for the beam with and without the elastic foundation

The values of critical loads for the beam without the elastic foundation increase with the increase of k_0 parameter. In other words, the sensitivity of beam to buckling decreases with the increase of volume fraction of the sandwich part. The longer the L_s part of the beam, the higher the obtained values of $\overline{F_{0,\mathrm{CR}}}$. For the beam resting on elastic foundation, the situation is similar. The critical loads increase with the increase of k_0 parameter values. With a further increase of k_0 parameter, the critical load increases smoothly.

The values of critical loads are higher for the two-part beam resting on Winkler's elastic foundation. This is in accordance with the results known from

work [35] and other literature sources. The loss of stability affects the displacement of Winkler's foundation. One can state that the relation between buckling and deformation of the elastic foundation is meaningful, and so is the relation between elastic foundation parameters and critical loads values. Moreover, the geometrical parameters (the values of L_0 and L_s) also play a significant role in buckling response of the beam.

3.2. Numerical studies

The numerical studies on two-part beam on Winkler's elastic foundation started with the study on convergence and validation to check the correctness of solution. Simply supported two-part beam was taken into the consideration in finite element analysis. Variable elastic foundation parameters were introduced to the calculations. Mechanical and geometrical parameters had the same values as those used in Section 3.1.

A numerical model was prepared. Finite element analysis was performed with the use of SolidWorks software for the beam with the same boundary conditions as those used for the analytical studies. The beam was composed of two parts: a rigid part, and a sandwich three-layered part, in agreement with parameters shown in Section 3.1. Both parts were modeled as solid bodies with a bonded contact. On the left end of the beam, there were fixed displacements in y and z directions, perpendicular to the x beam axis (roller support). On the right end of the beam, additional axis displacement was fixed (fixed support). The load was applied to the left end of the beam in the axis direction. Winkler's foundation was replaced by a system of discrete elastic supports.

Second-order elements in a form of tetrahedrons (10 nodes) were applied in the numerical investigations. The entire model was built of 608 938 nodes having 430 245 elements, for which mesh convergence was achieved. The maximum size of elements was set to 1.5 mm. The obtained results for variable sets of parameters are presented in Table 2.

Table 2. Results of numerical studies for variable beam parameters

Beam	Beam no. 1	Beam no. 2	Beam no. 3	Beam no. 4	Beam no. 5
λ_s	15.0	17.5	20.0	22.5	25.0
k_0	2/3	3/7	1/4	1/9	0
$F_{0,\mathrm{CR}}$ [kN] no foundation	20.686	17.821	16.295	15.638	15.465
$F_{0,\mathrm{CR}}$ [kN] with foundation	33.914	31.008	29.436	28.289	28.214

The numerical analysis focused on linear buckling of the beam. The main objective of the studies presented in this Section was to find the values of critical

loads as well as the buckling modes. The calculations were applied to a family of beams (elastic range) with various parameters. The values of critical loads were obtained and compared with analytical results based on Eq. (25).

The numerical results obtained for the two-part beam on Winkler's elastic foundation were compared to the analytical ones. These are presented in Fig. 4. The values of critical buckling loads in the two-part beam are influenced by the presence of Winkler's foundation and depend on geometric (variable values of λ_s and k_0) and mechanical parameters.

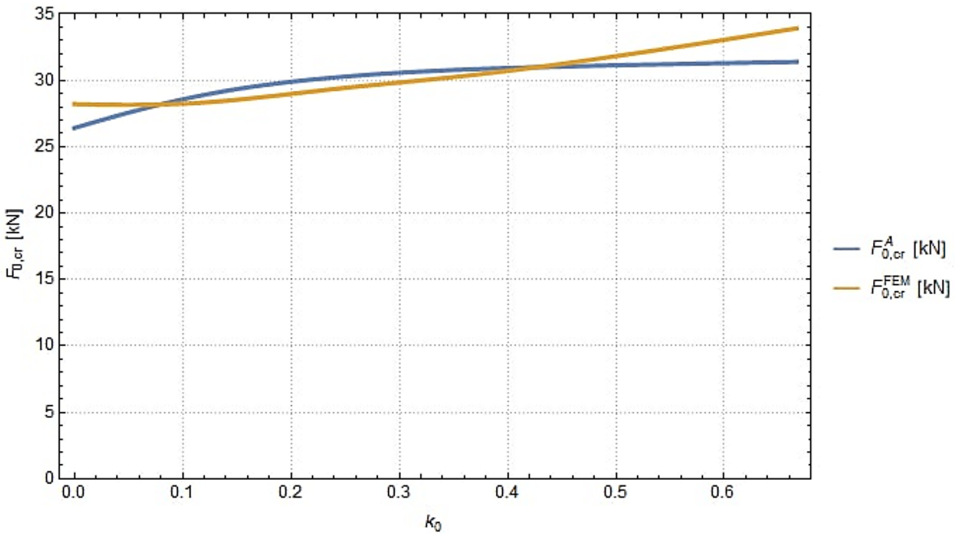

Fig. 4. The values of critical loads for two-part beam on elastic foundation with variable properties obtained with the use of analytical and numerical solution

The numerical values of critical loads for the beam without the elastic foundation increase with the increase of k_0 parameter. The same situation can be observed for the beam with Winkler's foundation. The increase of sandwich part length induces the increase of $\overline{F}_{0,\mathrm{CR}}$ values.

The numerical analysis confirmed previous assumptions. The critical buckling loads reach higher values for the beam resting on elastic foundation. The maximum value of relative difference between analytical and numerical results does not exceed 8% for B-1 beam. The low differences between the results prove the correctness of the proposed mathematical model presented in Section 2.

Sample solution for B-1 beam with a normalized amplitude is presented in Fig. 5. This buckling example confirms that neither elastic foundation parameters, nor geometric parameters of the two-part beam change the buckling shape in a significant way. The buckling load is the only variable parameter.

Linear buckling of the beam is strictly associated with the parameters of elastic foundation and the parameters of the two-part beam. Their values (obtained both

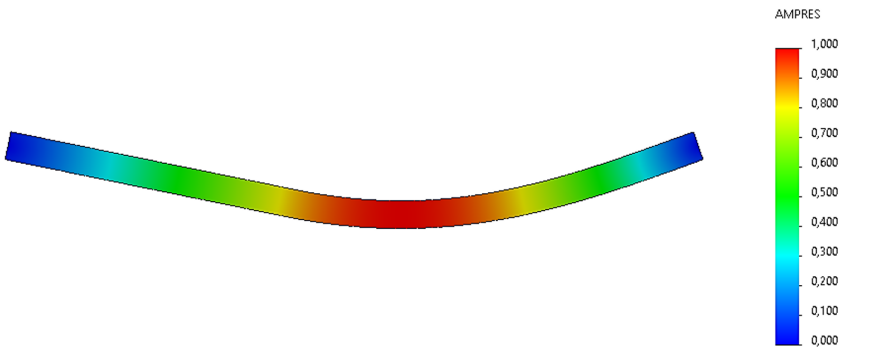

Fig. 5. Buckling mode for B-1 beam

analytically and numerically) increase with the increase of sandwich part length. The proposed analysis allows one to describe buckling characteristics for complex structures on elastic foundation.

4. Conclusions

The main objective of the presented work was the buckling analysis of an axially compressed two-part beam on Winkler's elastic foundation. The studies aimed to determine the influence of elastic foundation as well as geometry of the beam on critical loads values and the buckling shape. The beam consisted of a rigid homogeneous part and a sandwich three-layered structure. The mathematical model prepared by the authors demonstrated a good agreement with numerical studies.

Main conclusions from this work are as follows:

- In the case of beam without the elastic foundation, the values of critical loads increase with the increase of k_0 parameter. The same situation can be observed for the structure resting on Winkler's foundation.
- The values of critical loads (from both analytical and numerical solutions) are higher for the two-part beam resting on Winkler's elastic foundation.
- The values of critical buckling loads in a two-part beam are associated with the application of Winkler's foundation and depend on geometric (variable values of λ_s and k_0) and mechanical parameters.

The comparative analysis indicated good agreement between the analytical results and numerical calculations. The difference between mathematical solutions and the values obtained with the use of numerical method did not exceed 8%.

Acknowledgements

The paper is developed based on the scientific activity of the Łukasiewicz Research Network – Poznan Institute of Technology, and the statutory activity of the Poznan University of Technology (Grant of the Ministry of Science and Higher Education in Poland no. 0612/SBAD/3628).

References

[1] E. Magnucka-Blandzi and K. Magnucki. Effective design of a sandwich beam with a metal foam core. *Thin-Walled Structures*, 45(4):432–438, 2007. doi: 10.1016/j.tws.2007.03.005.

[2] K. Magnucki, P. Jasion, W. Szyc, and M.J. Smyczyński. Strength and buckling of a sandwich beam with thin binding layers between faces and a metal foam core. *Steel and Composite Structures*, 16(3):325–337, 2014. doi: 10.12989/scs.2014.16.3.325.

[3] T.-K. Nguyen, T.P. Vo, B.-D. Nguyen, and J. Lee. An analytical solution for buckling and vibration analysis of functionally graded sandwich beams using a quasi-3D shear deformation theory. *Composite Structures*, 156:238–252, 2016. doi: 10.1016/j.compstruct.2015.11.074.

[4] K. Magnucki, E. Magnucka-Blandzi, J. Lewiński, and S. Milecki. Analytical and numerical studies of an unsymmetrical sandwich beam – bending, buckling and free vibration. *Engineering Transactions*, 67(4):491–512, 2019. doi: 10.24423/EngTrans.1015.20190725.

[5] J. Liu, B. He, W. Ye, and F. Yang. High performance model for buckling of functionally graded sandwich beams using a new semi-analytical method. *Composite Structures*, 262:113614, 2021. doi: 10.1016/j.compstruct.2021.113614.

[6] Y.-H. Chen, and C.-D. Chen. Linear static, geometric nonlinear static and buckling analyses of sandwich composite beams based on higher-order refined zigzag theory. *Composite Structures*, 339:118131, 2024. doi: 10.1016/j.compstruct.2024.118131.

[7] M. Lezgy-Nazargah, A. Karamanli, and T.P. Vo. Bending, buckling and free vibration analyses of shallow-to-deep FG curved sandwich beams using a global-local refined shear deformation theory. *Structures*, 52:568–581, 2023. doi: 10.1016/j.istruc.2023.04.008.

[8] S.D. Pham, A. Karamanli, N. Wattanasakulpong, and T.P. Vo. A Quasi-3D theory for bending, vibration and buckling analysis of FG-CNTRC and GPLRC curved beams. *Structures*, 63:106431, 2024. doi: 10.1016/j.istruc.2024.106431.

[9] R. Khorramabadi, and S. Besharat Ferdosi. Post-buckling and vibration analysis of double-curved sandwich panels with SMA embedded faces. *Composites Part C: Open Access*, 12:100419, 2023. doi: 10.1016/j.jcomc.2023.100419.

[10] R. Kiran Kumar Reddy, A.R. Veerappan, N. George, and V. Bhagat. Thermo-mechanical buckling and sound radiation characteristics of 3D graphene porous core curved sandwich panels with composite facings. *Thin-Walled Structures*, 199:111753, 2024. doi: 10.1016/j.tws.2024.111753.

[11] M. Sobhy. Buckling and vibration of FG graphene platelets/aluminum sandwich curved nanobeams considering the thickness stretching effect and exposed to a magnetic field. *Results in Physics*, 16:102856, 2020. doi: 10.1016/j.rinp.2019.102865.

[12] Y. Zhai, J. Ma, Y. Yan, Q. Li, S. Wang, and G. Wang. Thermal buckling and free vibration of composite sandwich curved panels. *Composite Structures*, 267:113869, 2021. doi: 10.1016/j.compstruct.2021.113869.

[13] T. Quoc Quan, N. Huy Cuong, and N. Dinh Duc. Nonlinear buckling and post-buckling of eccentrically oblique stiffened sandwich functionally graded double curved shallow shells. *Aerospace Science and Technology*, 90:169–180, 2019. doi: 10.1016/j.ast.2019.04.037.

[14] P. Van Lieu, A.M. Zenkour, and G.T. Luu. Static bending and buckling of FG sandwich nanobeams with auxetic honeycomb core. *European Journal of Mechanics - A/Solids*, 103:105181, 2024. doi: 10.1016/j.euromechsol.2023.105181.

[15] G. Di Cara, M. D'Ottavio, and O. Polit. Variable kinematics finite plate elements for the buckling analysis of sandwich composite panels. *Composite Structures*, 330:117856, 2024. doi: 10.1016/j.compstruct.2023.117856.

[16] C. Aparecida Diniz, D. Brighenti Bortoluzzi, J.L. Junho Pereira, S. Simões da Cunha Jr, and G. Ferreira Gomes. On the influence of manufacturing parameters on buckling and modal properties of sandwich composite structures. *Structures*, 46:664–680, 2022. doi: 10.1016/j.istruc.2022.10.059.

[17] E. Madenci, Y.O. Özkılıç, A. Bahrami, C. Aksoylu, M. Rizal, M. Asyraf, I.Y. Hakeem, A.N. Beskopylny, S.A. Stel'makh, E.M. Shcherban, and S. Fayed. Experimental investigation and analytical verification of buckling of functionally graded carbon nanotube-reinforced sandwich beams. *Heliyon*, 10(8):e28388, 2024. doi: 10.1016/j.heliyon.2024.e28388.

[18] R. Patil, S. Joladarashi, and R. Kadoli. Effect of porosity and viscoelastic boundary conditions of FG sandwich beams in thermal environment: Buckling and vibration studies. *Structures*, 56:105001, 2023. doi: 10.1016/j.istruc.2023.105001.

[19] P. Cao and K. Niu. New unified model of composite sandwich panels/beams buckling introducing interlayer shear effects. *Composite Structures*, 252:112722, 2020. doi: 10.1016/j.compstruct.2020.112722.

[20] Z. Chen, J. Li, L. Sun, and L.-Y. Li. Flexural buckling of sandwich beams with thermal-induced non-uniform sectional properties. *Journal of Building Engineering*, 25:100782, 2019. doi: 10.1016/j.jobe.2019.100782.

[21] K. Mhada and O. Bourihane. A multi-scale model for global buckling and local wrinkling interaction with application to sandwich beams. *Structures*, 32:1398–1407, 2021. doi: 10.1016/j.istruc.2021.03.042.

[22] S. Waddar, J. Pitchaimani, M. Doddamani, and E. Barbero. Buckling and vibration behaviour of syntactic foam core sandwich beam with natural fiber composite facings under axial compressive loads. *Composites Part B: Engineering*, 175:107133, 2019. doi: 10.1016/j.compositesb.2019.107133.

[23] D. Lanc, T.P. Vo, G. Turkalj, and J. Lee. Buckling analysis of thin-walled functionally graded sandwich box beams. *Thin-Walled Structures*, 86:148–156, 2015. doi: 10.1016/j.tws.2014.10.006.

[24] Z. Kiral, M.E. Toygar, B.G. Kiral, and O. Sayman. Effect of the root crack on the lateral buckling loads and natural frequencies of sandwich composite beams. *Composites Part B: Engineering*, 53:308–313, 2013. doi: 10.1016/j.compositesb.2013.04.060.

[25] A. Karamanli and M. Aydogdu. Buckling of laminated composite and sandwich beams due to axially varying in-plane loads. *Composite Structures*, 210:391–408, 2019. doi: 10.1016/j.compstruct.2018.11.067.

[26] K.Y. Volokh and A. Needleman. Buckling of sandwich beams with compliant interfaces. *Computers & Structures*, 80(14-15):1329–1335, 2002. doi: 10.1016/S0045-7949(02)00076-7.

[27] P. Zhang, P. Schiavone, and H. Qing. Stress-driven local/nonlocal mixture model for buckling and free vibration of FG sandwich Timoshenko beams resting on a nonlocal elastic foundation. *Composite Structures*, 289:115473, 2022. doi: 10.1016/j.compstruct.2022.115473.

[28] H. Nguyen Thi. On mechanical behavior of two-layer functionally graded sandwich curved beams resting on elastic foundations using an analytical solution and refined Timoshenko beam theory. *Ain Shams Engineering Journal*, 13(4):101674, 2022. doi: 10.1016/j.asej.2021.11.016.

[29] T. Fu, Z. Chen, H. Yu, C. Li, and Y. Zhao. Thermal buckling and sound radiation behavior of truss core sandwich panel resting on elastic foundation. *International Journal of Mechanical Sciences*, 161-162:105055, 2019. doi: 10.1016/j.ijmecsci.2019.105055.

[30] F. Abbaspour, and H. Arvin. Thermo-electro-mechanical buckling analysis of sandwich nanocomposite microplates reinforced with graphene platelets integrated with piezoelectric facesheets resting on elastic foundation. *Computers & Mathematics with Applications*, 101:38–50, 2021. doi: 10.1016/j.camwa.2021.09.009.

[31] M. Song, L. Chen, J. Yang, W. Zhu, and S. Kitipornchai. Thermal buckling and postbuckling of edge-cracked functionally graded multilayer graphene nanocomposite beams on an elastic foundation. *International Journal of Mechanical Sciences*, 161-162:105040, 2019. doi: 10.1016/j.ijmecsci.2019.105040.

[32] V.D. Quang, T.Q. Quan, and P. Tran. Static buckling analysis and geometrical optimization of magneto-electro-elastic sandwich plate with auxetic honeycomb core. *Thin-Walled Structures*, 173:108935, 2022. doi: 10.1016/j.tws.2022.108935.

[33] V. Kumar, S.J. Singh, V.H. Saran, and S.P. Harsha. Effect of elastic foundation and porosity on buckling response of linearly varying functionally graded material plate. *Structures*, 55:1186–1203, 2023. doi: 10.1016/j.istruc.2023.06.084.

[34] Y. Chai, Z. Song, and F. Li. Investigations on the influences of elastic foundations on the aerothermoelastic flutter and thermal buckling properties of lattice sandwich panels in supersonic airflow. *Acta Astronautica*, 140:176–189, 2017. doi: 10.1016/j.actaastro.2017.08.016.

[35] I. Wstawska, K. Magnucki, and P. Kędzia. Stability of three-layered beam on elastic foundation. *Thin-Walled Structures*, 175:109208, 2022. doi: 10.1016/j.tws.2022.109208.

[36] Y. Yang, B. Chen, W. Lin, Y. Li, and Y. Dong. Vibration and symmetric thermal buckling of asymmetric annular sandwich plates with piezoelectric/GPLRC layers rested on foundation. *Aerospace Science and Technology*, 110:106495, 2021. doi: 10.1016/j.ast.2021.106495.

[37] Y. Lv, J. Zhang, and L. Li. Thermal buckling and postbuckling of functionally graded multilayer GPL-reinforced composite beams on nonlinear elastic foundations. *Heliyon*, 9(9):e19549, 2023. doi: 10.1016/j.heliyon.2023.e19549.

[38] X. Chen, H.-S. Shen, and C. Li. Re-examination of nonlinear vibration, nonlinear bending and thermal postbuckling of porous sandwich beams reinforced by graphene platelets. *Composite Structures*, 322:117392, 2023. doi: 10.1016/j.compstruct.2023.117392.

[39] Q. Li, D. Wu, X. Chen, L. Liu, Y. Yu, and W. Gao. Nonlinear vibration and dynamic buckling analyses of sandwich functionally graded porous plate with graphene platelet reinforcement resting on Winkler-Pasternak elastic foundation. *International Journal of Mechanical Sciences*, 148:596–610, 2018. doi: 10.1016/j.ijmecsci.2018.09.020.

[40] H. Babaei. Thermomechanical analysis of snap-buckling phenomenon in long FG-CNTRC cylindrical panels resting on nonlinear elastic foundation. *Composite Structures*, 286:115199, 2022. doi: 10.1016/j.compstruct.2022.115199.

[41] X. Chang, J. Zhou, and Y. Li. Post-buckling characteristics of functionally graded fluid-conveying pipe with geometric defects on Pasternak foundation. *Ocean Engineering*, 266(4):113056, 2022. doi: 10.1016/j.oceaneng.2022.113056.

[42] A.H. Sofiyev and N. Kuruoglu. Buckling analysis of shear deformable composite conical shells reinforced by CNTs subjected to combined loading on the two-parameter elastic foundation. *Defence Technology*, 18(2):205–218, 2022. doi: 10.1016/j.dt.2020.12.007.

[43] C.R. Briscoe, S.C. Mantell, and J.H. Davidson. Shear buckling in foam-filled web core sandwich panels using a Pasternak foundation model. *Thin-Walled Structures*, 48(6):460–468, 2010. doi: 10.1016/j.tws.2009.12.005.

[44] Z. Wang and G. Yao. Nonlinear vibration and stability of sandwich functionally graded porous plates reinforced with graphene platelets in subsonic flow on elastic foundation. *Thin-Walled Structures*, 194(A):111327, 2024. doi: 10.1016/j.tws.2023.111327.

[45] P. Kozić, R. Pavlović, and D. Karličić. The flexural vibration and buckling of the elastically connected parallel-beams with a Kerr-type layer in between. *Mechanics Research Communications*, 56:83–89, 2014. doi: 10.1016/j.mechrescom.2013.12.003.

[46] J. Guo, T. Sun, and E. Pan. Three-dimensional nonlocal buckling of composite nanoplates with coated one-dimensional quasicrystal in an elastic medium. *International Journal of Solids and Structures*, 185-186:272–280, 2020. doi: 10.1016/j.ijsolstr.2019.08.033.

[47] P. Jasion and K. Magnucki. Global buckling of a sandwich column with metal foam core. *Journal of Sandwich Structures & Materials*, 15(6):718–732, 2013. doi: 10.1177/1099636213499339.